Hyperfine excitation of NS + due to para-H 2 (j = 0) impact

Cheikh Tidiane Bop

MNRAS **000**, 1–?? (2019) Preprint 13 June 2019 Compiled using MNRAS LATEX style file v3.0

Hyperfine excitation of NS^+ due to para-$H_2(j = 0)$ impact

Cheikh T. Bop★

Laboratory of Atoms Lasers, Departement of Physics, Faculty of Science and Technique, University Cheikh Anta Diop of Dakar, 5005, Senegal

LOMC- UMR 6294, CNRS- Université du havre, 25 rue Philippe Lebon, BP 1123, F-76063 Le Havre, France.

Accepted XXX. Received YYY; in original form ZZZ

ABSTRACT

Sulfur bearing nitrogenous compounds have been observed in space over this last decade. Modeling their abundances has been done using rate coefficients of isoelectronic molecules. In order to satisfy the astrophysical precision required, we report the actual rate coefficients of NS^+ induced by collision with the most abundant interstellar species (para-H_2). Considering the 23 low-lying rotational levels of NS^+, we were able to compute the (hyperfine) rate coefficients up to 100 K. These latter were carried out by averaging cross sections over the Maxwell-Boltzmann velocity distribution. The state-to-state inelastic cross sections were determined in the quantum mechanical close coupling approach for total energies ranging up to 1,400 cm^{-1}. These dynamic data result from a four dimensional potential energy surface (4D-PES) which was spherically averaged over the H_2 orientations. The 4D-PES was calculated using the the explicitly correlated coupled cluster method with simple, double and non-iterative triple excitation (CCSD(T)–F12) connected to the augmented–correlation consistent–polarized valence triple zeta Gaussian basis set (aug–cc–pVTZ). The so-averaged PES presents a very deep well of 596.72 cm^{-1} at $R = 5.94\ a_0$ and $\theta_1 = 123.20°$. Discussions on the propensity rules for the (hyperfine) rate coefficients were made and they are in favor of $(\Delta j = \Delta F)\ \Delta j = 1$ transitions. The results presented here may be crucially needed in order to accurately model the NS^+ abundance in space. In addition, we expect that this paper will encourage investigations on the sulfur bearing nitrogenous compounds.

Key words: ISM: molecules – molecular data – molecular processes – ISM : abundances

1 INTRODUCTION

Atomic nitrogen (N) is among the most abundant species in the interstellar medium (ISM). It is also known as a key element in the production of precursors for the formation of interstellar prebiotic molecules. In astrobiology, nitriles are suspected to play an important role in the prebiotic chemistry which preceded the presence of life on Earth. However, the partitioning of elemental nitrogen significantly affects its chemistry in the ISM (Daranlot et al. 2012; Meyer et al. 1997). In fact, molecular nitrogen (N_2) is unobservable in radioastronomy as it has no permanent electric dipole moment. Therefore, diazenylium (or protonated molecular nitrogen N_2H^+) and its deuterated isotope are generally used to probe the abundance of N_2 (Daniel et al. 2013). Nevertheless, nitrogen is not the only abundant interstellar element with a poorly understood chemistry. Indeed, sulfur (S) severely depletes in molecular clouds (Prasad & Huntress Jr 1982; Tieftrunk et al. 1994; Wakelam et al. 2004). The use of a depleted value ($\leq 1\%$) relative to the S-cosmic abundance, when modeling the dense interstellar environments, has led to a chemistry weakly understood (Laas & Caselli 2019). Therefore, nitrogenous compounds containing sulfur constitute a clue to constrain simultaneously the chemistry of both atoms mentioned above.

Nowadays, more than 200 molecules are observed in the ISM and among them only 4 contain both nitrogen and sulfur atoms (these latter will be thereafter denoted as [N,S]-bearers). Isothiocyanic acid (HNCS) was observed towards Sgr B2 from its rotational emission lines ($j + 1 \rightarrow j$, with $j = 6 - 8, 10$ and 11). This led to a HNCS column density of $\sim 10^{13} cm^{-2}$ (Frerking et al. 1979). Later, Halfen et al. (2009) reported the detection of its isomer, namely thiocyanic acid (HSCN) using the Arizona Radio Observatory (ARO) 12 m telescope. For each isomer HSCN and HNCS, they derived an abundance in Sgr B2 relative to molecular hydrogen (H_2) of 4.5×10^{-12} and 1.1×10^{-11} respectively. Despite the stability difference among these latter, HNCS lies at $\sim$ 2,090 cm^{-1} below HSCN (Durig et al. 2006; Wierzejewska & Moc 2003), Halfen et al. (2009) estimated an abundance ratio (HNCS/HSCN) of only $\sim$ 2.44 in Sgr B2(N). Moreover, the diatomic nitrogen sulfide (NS) is widespread in space. Indeed, it was first detected towards the Sgr B2 via its $5/2 \rightarrow 3/2$ transition in radio emission (Gottlieb et al. 1975). In the same region, Kuiper et al. (1975) ob-

★ cheikhtidiane.bop@ucad.edu.sn

served the $5/2 \rightarrow 3/2$ millimeter-wavelength radiation. McGonagle & Irvine (1997) recorded several fine rotational emission lines of NS towards 12 out of the 14 observed giant molecular clouds. In addition, NS was also detected in the coma of the Hale Bopp comet with the James Clerk Maxwell Telescope (JCMT) (Irvine et al. 2000). More recently, NS^+ was observed via its $2 \rightarrow 1$ transition in prestellar cores, cold molecular clouds, and shocks using the Institut de Radioastronomie Millimétrique (IRAM) 30 m telescope (Cernicharo et al. 2018). Due to its omnipresence towards the dark clouds of different evolutionary stages, NS^+ is expected to be a good tracer for the chemical and physical conditions in these environments. It is worth noting that 2 out of 4 interstellar [N,S]-containing molecules were identified during this last decade making them the target of several recent experimental and theoretical investigations (Krupa & Wierzejewska 2016; Brünken et al. 2009; Pereira et al. 2009).

The early detected [N,S]-bearers did not revive interest in the frame of rotational energy transfer. Thus, Cernicharo et al. (2018) relied on the CS rotational rate coefficients and a series of approximations to compute the abundance ratio (NS/NS^+). However, the collisional rates of HSN and HNS which are likely present in the ISM (but not yet observed) were reported by Ajili et al. (2016a) and Ajili et al. (2016b) respectively. In contrast, the NS^+ rate coefficients are widely studied, thanks to its omnipresence in the ISM. Indeed, Trabelsi et al. (2018) reported pure rotational rate coefficients of NS^+ induced by collision with helium (He). Since Cernicharo et al. (2018) detected hyperfine transitions of NS^+ as well, Cabrera-González et al. (2018) computed the corresponding rates due to He impact. These authors discussed the approximation made by Cernicharo et al. (2018) in the calculation of the NS^+ abundance but the conclusions of Trabelsi et al. (2018) and those of Cabrera-González et al. (2018) disagree. In fact, Trabelsi et al. (2018) validated the fact of scaling up by 5 the CS rate coefficients to derive those of NS^+ while Cabrera-González et al. (2018) highlighted the limits of such procedures.

It is worth mentioning that abundance ratio calculations require high accurate rate coefficients induced by collision with molecular hydrogen (H_2) which is the main collision partner in the ISM (Hernández Vera et al. 2017). Such collisional data can be approximated, with a scaling factor by mean of those obtained using He as collision partner, since both para-$H_2(j = 0)$ and He are closed shell species containing two electrons. However, the efficiency of such a methodology is discussed in the literature mainly for charged compounds such as NS^+. Indeed, based on HCO^+ Monteiro (1985) suggested the use of a scaling factor of $2 - 4$ while recently Lanza et al. (2014b) via HCl pointed the inaccuracy of using a scaling factor. These two items along with the fact that rules which stem from hydrides may not be general led us consider in this paper the collision of NS^+ by para-$H_2(j = 0)$.

In media where NS^+ were observed, the temperature is relatively low ($T < 100\ K$) making that molecular hydrogen remains mainly in its fundamental rotational state, in other word in the form para-$H_2(j = 0)$. Indeed, the first excited energy level of para-H_2 lies at about 520 K above the ground state (Huber 2013). In addition, para-$H_2(j = 0)$ is rigorously spherically symmetric and thus can be unambiguously considered as a spherical particle (see Li et al. (2010) and references therein). Such an approximation will significantly reduce the computational efforts. In fact, charged species strongly interact with He (Bop et al. 2016, 2017, 2018) and then much more with H_2 leading to very deep potential wells. Such well depths supplemented by the low rotational constant of NS^+ (~ 0.83 (Cernicharo et al. 2018)) would make the dynamic calculations computationally expensive.

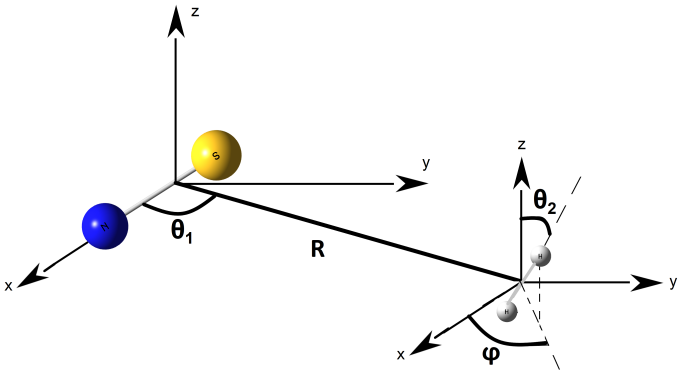

Figure 1. Definition of the body-fixed coordinate system, $\theta_1 = 0$ corresponds to the $H_2 \cdots NS^+$ linear configuration.

This work will be presented as follows: Section 2 describes the electronic calculations, Section 3 presents the dynamic results and finally in Section 4 are detailed the concluding remarks.

2 POTENTIAL ENERGY SURFACE

The complexes cis-($HNSH^+$), trans-($HNSH^+$) and H_2NS^+ lie at 11 $Kcal$ (3,850 cm^{-1}), 13 $Kcal$ (4,550 cm^{-1}) and 29 $Kcal$ (10,100 cm^{-1}) respectively below the H_2–NS^+ dissociation limit (Nguyen et al. 1994). Thus, these reactive channels can be neglected while treating the rotational collisions. Indeed, in this work the largest scattering energy is set to 1,400 cm^{-1}.

The potential energy surface presented in this paper stems from the interactions among two linear molecules in their ground electronic state, namely $NS^+(^1\Sigma^+)$ and $H_2(^1\Sigma^+)$. Rigorously, this requires a determination of a full four-dimensional potential (4D-PES), $V(R,\theta_1,\theta_2,\varphi)$. The R-parameter describes the distance between the centers of mass of the colliding partners, θ_1 represents the collision direction and the couple (θ_2, φ) stands for the orientations of H_2 relative to the NS^+ body-fixed coordinate system (see Fig. 1). Nevertheless, in this work we reduced the freedom degrees by averaging the PESs calculated into the three main H_2 orientations, namely (θ_2, φ) = {(0°,0°); (90°,0°) and (90°,90°)}. Such a spherical average two-dimensional PES (sphe-ave-2D-PES) may lead to reliable dynamic results due to para-$H_2(j = 0)$ which is spherically symmetric. Indeed Kłos & Lique (2008), when using a limited PES with three H_2 orientations then a full 4D-PES, showed that sphe-ave-2D-PES can accurately describe the scattering of SiS with H_2. Therefore, numerous calculations were based on this approximation (Lique et al. 2008; Denis-Alpizar et al. 2013; Sahnoun et al. 2018). However, it is worth noting that the closed channel $j = 2$ of H_2 would lead to relative errors of 10–50% (Walker et al. 2016; Dumouchel et al. 2011; Lanza et al. 2014a; Dubernet & Grosjean 2002).

The PES was constructed using the H_2 and NS^+ bond lengths which were held fixed at their vibrationally averaged experimental distances $\langle r_{H_2} \rangle_0 = 1.449\ a_0$ (Huber 2013) and $\langle r_{NS^+} \rangle_0 = 2.7189\ a_0$ (Cernicharo et al. 2018). Hereafter for each couple (θ_2, φ), R and θ_1 were assigned to 48 and 19 values respectively leading to an overall of 2,736 geometries. More explicitly, θ_1 was varied using a regular step of 10° while the R-spacing was set to

0.25 a_0 for 4 $\leqslant R \leqslant$ 10 a_0, 0.5 a_0 for 10 $\leqslant R \leqslant$ 15 a_0, 1 a_0 for 15 $\leqslant R \leqslant$ 25 a_0 and 25 a_0 for 25 $\leqslant R \leqslant$ 100 a_0. All these configurations were treated with the explicitly correlated coupled cluster method with single, double and non-iterative triple excitation (CCSD(T)-F12) (Knizia et al. 2009) in conjunction with the augmented-correlation consistent-polarized valence triple zeta Gaussian basis set (aug-cc-pVTZ) (Dunning Jr 1989). For further details on the methodology followed, see Bop et al. (2017). Such a level of theory (CCSD(T)-F12/au-cc-pVTZ) was used as implemented in the MOLPRO molecular package (Werner et al. 2010). The basis set superposition error was corrected using the counterpoise procedure of Boys & Bernardi (1970):

$$V(R,\theta_1,\theta_2,\varphi) = E_{NS^+-H_2}(R,\theta_1,\theta_2,\varphi) - E_{NS^+}(R,\theta_1,\theta_2,\varphi) - E_{H_2}(R,\theta_1,\theta_2,\varphi) \quad (1)$$

The so-computed PESs are represented in the Fig. 2. Panel *(a)* displays the interactions in the configuration where H_2 is perpendicular to the plane formed by the NS^+ bond and the collision axis, panel *(b)* [panel *(c)*] depicts the PES in the case H_2 belongs to the collision plane and parallel [perpendicular] to the NS^+ bond and panel *(d)* presents the sphe-ave-2D-PES. As one can see, all these configurations present large anisotropies with very deep potential wells. Indeed, one global minimum of 848.24 cm^{-1} is observed for the $V(R,\theta_1,\theta_2 = 0,\varphi = 0)$ at R = 5.76 a_0 and θ_1 = 123.20°. For the $V(R,\theta_1,\theta_2 = 90,\varphi = 0)$, the well depth is 769.60 cm^{-1} and it is located at R = 5.70 a_0 and θ_1 = 112.90°. Concerning the $V(R,\theta_1,\theta_2 = 90,\varphi = 90)$, two local minima of 210.96 cm^{-1} and 683.63 cm^{-1} are obtained. The shallower occurs at R = 7.40 a_0 and θ_1 = 33.58° while the deeper one stems for R = 6.52 a_0 and θ_1 = 180°. It is worth noting that the potentials drawn in panel *(b)* and panel *(c)* seem complementary by shape. In this realm, it is not surprising that the sphe-ave-2D-PES has typically the shape of $V(R,\theta_1,\theta_2 = 0,\varphi = 0)$. However the potential well is located at $\{\theta_1,R\}$ = {123.20°,5.94 a_0} and its depth is shifted to 596.72 cm^{-1}.

Furthermore, we compare in table 1 the global minima (V_{min}) of the NS^+–H_2 (this work) and NS^+–He (Trabelsi et al. 2018; Cabrera-González et al. 2018) PESs. Regarding the present work, θ refers to θ_1 and contrary to the previous works mentioned above, 0° corresponds to the $H_2 \cdots NS^+$ configuration. This implies to take into account the inversion symmetry for a reliable comparison, $V(R,\theta) = V(R,\pi-\theta)$. Thus, the global minimum obtained in this work would be observed at θ_1 = 56.8°. Concerning the R-distance, it is smaller for the NS^+–H_2 complex. Such a finding is not surprising if we call back the H_2 bond length (1.449 a_0) effects in the distances between the atoms of the system. Therefore, the agreements among the PESs are geometrically good but as expected the well depths are very different $V_{min}(NS^+-H_2) \sim = 3.8 \times V_{min}(NS^+-He)$. It is stated in the introduction that the interactions with molecular hydrogen are likely much more stronger than those due to helium. Based on these analysis, the potential presented here is quite reliable for dynamic calculations.

In order to derive the basic input required for the dynamic calculations, we expand the sphe-ave-2D-PES, $V(R,\theta_1)$, using a cubic spline interpolation routine over the Legendre polynomial functions including up to 19 radial coefficient (V_λ).

$$V(R,\theta_1) = \sum_{\lambda=0}^{\lambda_{max}} V_\lambda(R) P_\lambda(cos\theta_1) \quad (2)$$

Table 1. Comparison of the potential well (in unit of cm^{-1}) and the corresponding geometry of NS^+–H_2 computed in this work and those of NS^+–He previously reported.

R (a_0)	θ (°)	This work	Previous NS^+–He PESs	
5.94	123.20	596.72	—	—
6.10	57.00	—	156.25[a]	—
6.16	53.50	—	—	154.80[b]

[a] stands for Trabelsi et al. (2018)
[b] stands for Cabrera-González et al. (2018)

Table 2. Spectroscopic constants of NS^+ and the parameters of the log derivative propagator used to solve for the coupled equations.

B_0 = 0.835 cm^{-1}[a]	j_{max} = 16 – 30
D_0 = 1.17 × 10^{-6} cm^{-1}[a]	STEPS =30, 10
μ = 1.931 au	R_{min}, R_{max} = 2, 95 a_0
$DTOL$ = 0.1 $Å^2$	$OTOL$ = 0.001 $Å^2$

[a] stands for Cernicharo et al. (2018)

3 DYNAMIC CALCULATIONS

In this paper we focus on the hyperfine rotational rate coefficients of NS^+ since such transitions were observed in the ISM (Cernicharo et al. 2018). As the rigid-rotor approximation was used in the construction of the PES, the largest total energy (E) used in the calculations of the cross sections was set to 1,400 cm^{-1} below the excited vibrational levels which are governed by the vibrational constant w_e = 1415 ± 20 cm^{-1} (Dyke 1977).

3.1 Cross sections

The exact quantum mechanical close coupling method (CC) developed by Arthurs & Dalgarno (1960) was employed as it is implemented in the MOLSCAT code (Hutson & Green 1994) to compute the state-to-state integral inelastic cross sections. The coupled equations were solved by mean of the log derivative propagator (Manolopoulos 1986). This latter depends on some parameters which were defined by performing convergence tests. Briefly, the integrations were carried out among 2 and 95 a_0 using a fine step which is governed by the STEPS-parameter. These parameters along with the reduced mass (μ) of NS^+–H_2 and the spectroscopic constants (B_0 and D_0) of NS^+ are reported in table 2. In addition, the rotational basis was set large enough (including rotational levels up to j_{max} = 30) and the convergence criteria were defined by setting the diagonal and off-diagonal tolerances to $DTOL$ = 0.1 $Å^2$ and $ODTOL$ = 0.001 $Å^2$. In order to correctly describe the resonances, a tight energy grille which was smoothly increased over a wide range, was necessary as the potential well is deep. Typically, the step was fixed at 0.1 cm^{-1} for 1.7 $\leq E \leq$ 100.0 cm^{-1}, 0.2 cm^{-1} for 100.2 $\leq E \leq$ 200.0 cm^{-1}, 0.5 cm^{-1} for 200.5 $\leq E \leq$ 300.0 cm^{-1}, 1 cm^{-1} for 301 $\leq E \leq$ 500 cm^{-1}, 2 cm^{-1} for 502 $\leq E \leq$ 600 cm^{-1}, 5 cm^{-1} for 605 $\leq E \leq$ 800 cm^{-1}, 10 cm^{-1} for 810 $\leq E \leq$ 1,000 cm^{-1} and 25 cm^{-1} for 1,025 $\leq E \leq$ 1,400 cm^{-1}.

Fig. 3 displays the variation of the rotational de-excitation cross sections of NS^+, induced by collision with para-H_2(j = 0), as a function of the kinetic energy (E_k). In both panels, the Feshbach and shape resonances are visible for energies up to 200 cm^{-1}. In addition, a broad shape resonance is seen at 300 – 600 cm^{-1}. Such a wide resonance width is due to the deep potential well. More explicitly, the Feshbach resonances present large amplitudes (for $E_k \leq$ 70 cm^{-1}) which slowly decrease relative to the kinetic en-

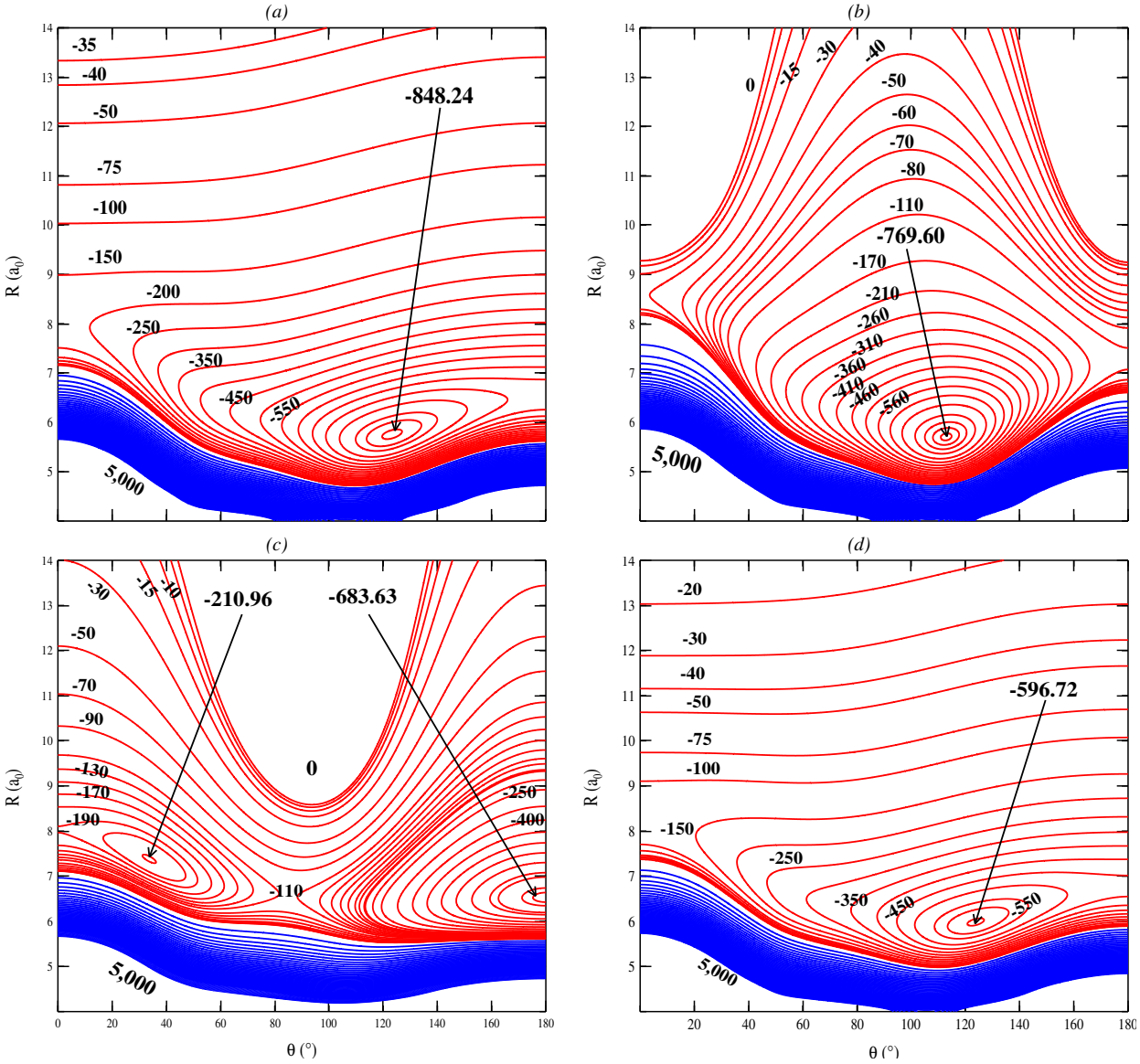

Figure 2. Two-dimensional potential energy surfaces of the NS^+–H_2 system (in unit of cm^{-1}): panel *(a)* corresponds to $V(R, \theta_1, \theta_2 = 0, \varphi = 0)$, panel *(b)* stands for $V(R, \theta_1, \theta_2 = 90, \varphi = 0)$, panel *(c)* describes the $V(R, \theta_1, \theta_2 = 90, \varphi = 90)$ and panel *(d)* depicts the sphe-ave-2D-PES. For the attractive part of the PES, the contours are labeled while a spacing of 100 cm^{-1} is used for the repulsive part.

ergy. Beyond 200 cm^{-1}, they almost disappear while the shape resonances persist. In fact, such behavior was expected as quasi-bound states form when the H_2 projectile is trapped in the potential well. Such interactions lead to Feshbach resonances which will persist until the H_2 projectile reaches enough energy to escape the trap (i.e to break the quasi-bound states). Otherwise, the shape resonances are governed by quasi-bound states due to tunneling effects through the centrifugal barrier. It is worth mentioning that beyond the wide range and large amplitudes of the resonances, the cross sections presented in this work are very similar to those computed by Trabelsi et al. (2018) and Cabrera-González et al. (2018), in terms of shape. From the upper panel of Fig. 3, one can see that the odd Δj transitions predominate as the $1 \rightarrow 0$ de-excitation outweighs in the whole energy range. This propensity rule will persist in the rotational rate coefficients.

3.2 Rate coefficients

The so-presented cross sections were thermally averaged using the Maxwell-Boltzmann velocity distribution to determine the close coupling rotational rate coefficients ($k^{CC}_{j \longrightarrow j'}$),

$$k^{CC}_{j \longrightarrow j'}(T) = \left(\frac{8}{\pi\mu\beta}\right)^{1/2} \beta^2 \int_0^\infty E_k \sigma(E_k) e^{-\beta E_k} \, dE_k \qquad (3)$$

where E_k stands for the kinetic energy and β is the reverse of the product $k_B \times T$ with k_B being the constant of Boltzmann. Based on the temperature range of the media were NS^+ was observed, we report rate coefficients corresponding to the 23 lowest rotational levels for temperatures up to 100 K. Thereafter, the hyperfine rate coefficients ($k^{IOS}_{j,F \longrightarrow j',F'}$), due to the nuclear spin of nitrogen ($I = 1$), can be computed using the free-spin close coupling rate coefficients mentioned above ($|j - I| \leq F \leq (j + I)$) (Faure & Lique 2012). This requires preliminary calculations of the fundamental

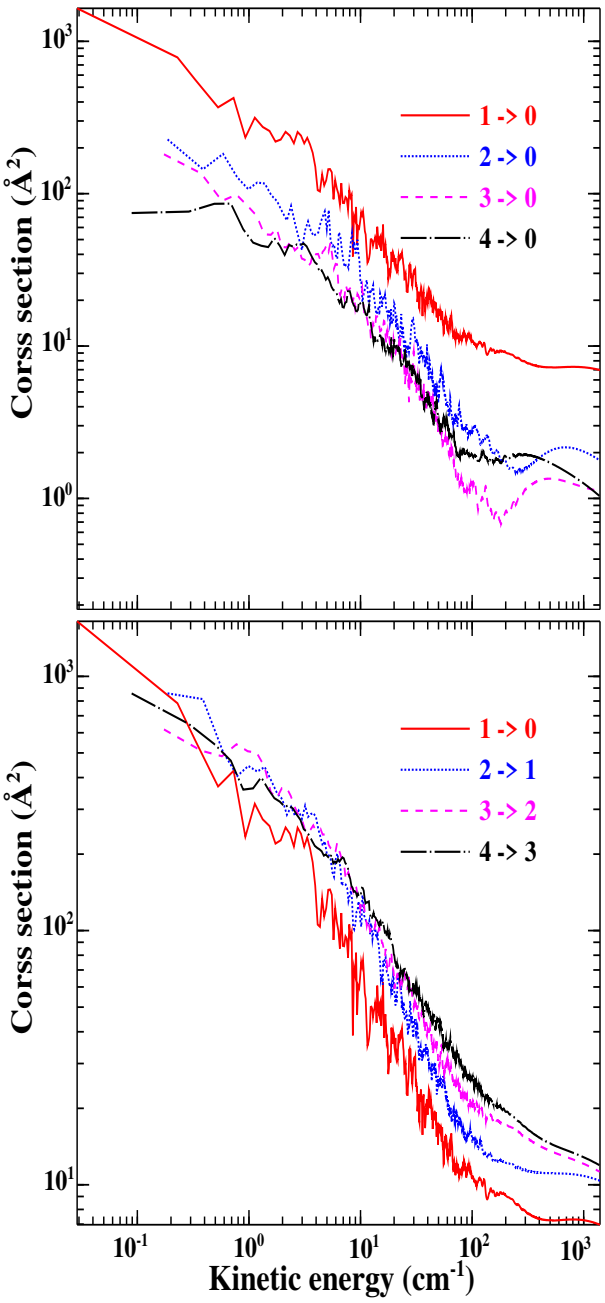

Figure 3. Rotational cross-sections of NS$^+$ induced by collision with para-H$_2$($j = 0$) as a function of the kinetic energy: the $j \longrightarrow 0$ transitions are represented in the upper panel and the transitions for which $\Delta j = 1$ are shown in the lower panel.

infinite order sudden (IOS) rate coefficients ($k_{0\longrightarrow L}$), the inelastic IOS rates ($k^{IOS}_{j\longrightarrow j'}$) (Goldflam et al. 1977), then the hyperfine IOS rate coefficients ($k^{ios}_{j,F\longrightarrow j',F}$). Typically, we followed step-by-step the algorithm below:

$$k^{IOS}_{j\longrightarrow j'}(T) = (2j'+1)\sum_L \begin{pmatrix} j' & j & L \\ 0 & 0 & 0 \end{pmatrix}^2 k_{0\longrightarrow L}(T) \qquad (4)$$

$$k^{ios}_{j,F\longrightarrow j',F'}(T) = (2j+1)(2j'+1)(2F'+1)\times \sum_L \begin{pmatrix} j' & j & L \\ 0 & 0 & 0 \end{pmatrix}^2 \begin{Bmatrix} j & j' & L \\ F' & F & I \end{Bmatrix}^2 k_{0\longrightarrow L}(T) \qquad (5)$$

$$k^{IOS}_{j,F\longrightarrow j',F'}(T) = \frac{k^{ios}_{j,F\longrightarrow j',F'}(T)}{k^{IOS}_{j\longrightarrow j'}(T)} \times k^{CC}_{j\longrightarrow j'}(T). \qquad (6)$$

In fact, the reliability of this approximative treatment has been assessed by comparing with the almost exact recoupling method which is based on the scattering matrix (see Faure & Lique (2012) for further discussions).

Fig.4 depicts the variation of the close coupling rate coefficients relative to the kinetic temperature for transitions involving the 8 low-lying rotational levels of NS$^+$. In the upper panel where the de-excitations ($j \longrightarrow 0$) are presented, the $1 \longrightarrow 0$ rotational transition strongly outweighs confirming the propensity previously observed in the cross sections. The lower panel presents a comparison among the dominant transitions ($\Delta j = 1$). As one can see, the $1 \longrightarrow 0$ transition is largely shifted below the other transitions. Globally, the magnitude of the rate coefficients increases when j increases and beyond $j = 4$, this pattern is reversed. This behavior is in perfect harmony with the observations as the dominant transitions (the transitions with large magnitudes at low temperature except $4 \longrightarrow 3$ and $6 \longrightarrow 5$, see the lower panel of Fig.4) were detected in the B1b prestellar core where the gas kinetic temperature is $10 - 15$ K (Cernicharo et al. 2018). Indeed, this work shows that these transitions exhibit large magnitudes at $T \leq 15$ K which lead to strong spectral line intensities. In addition, the $2 \longrightarrow 1$ emission line which was observed in several environments, making NS$^+$ ubiquitous, was not detected towards the Orion-KL hot cores where $T \geq 100$ K. Based on our work, this failure may stem from the fact that the magnitude of this transition decreases steadily ($\sim$ 50%) from $10 - 100$ K and becomes asymptotic beyond 100 K as shown by Trabelsi et al. (2018). It is noteworthy that, in terms of behavior, the data previously published by Trabelsi et al. (2018) and Cabrera-González et al. (2018) are similar to those worked out in this paper for $T \geq 20$ K. The discrepancy noted at lower temperatures is attributed to the numerous resonances observed here at low kinetic energies.

In order to better appreciate the disagreements mentioned above, we compare in table 3 [table 4] our data and those of Trabelsi et al. (2018) [Cabrera-González et al. (2018)]. In both tables, the brackets stand for the ratios of the rate coefficients (NS$^+$−para-H$_2$($j = 0$)/NS$^+$−He). The ratio observed in both tables 3 varies from 1.93 to 3.71 leading to expect an interval of about 2-4 for a complete set of comparison. This is in quite good agreement with the results of Monteiro (1985) who suggested to use a scaling factor of 2-4 in the aim of deriving rate coefficients due to para-H$_2$($j = 0$) from those induced by He. Moreover, involving the hyperfine splitting propagates the ratio out of the interval mentioned above. Indeed, table 4 shows that the ratio fluctuates between 1.47 and 3.70. Therefore as one can remark the ratio is not constant, instead, it depends on both of the transition and the temperature. However, it is worth mentioning that for a set of quasi-elastic transitions, the ratio varies only with respect to the temperature. More explicitly, at a fixed temperature and for $j = j'$, the ratio is held constant whatever the values of F and F'. Otherwise, agreements are observed for the propensity rules which are in favor of $\Delta j = \Delta F$ transitions. Despite the similar propensities, our finding globally prevents the fact of using He as template for para-H$_2$($j = 0$) in the case of charged

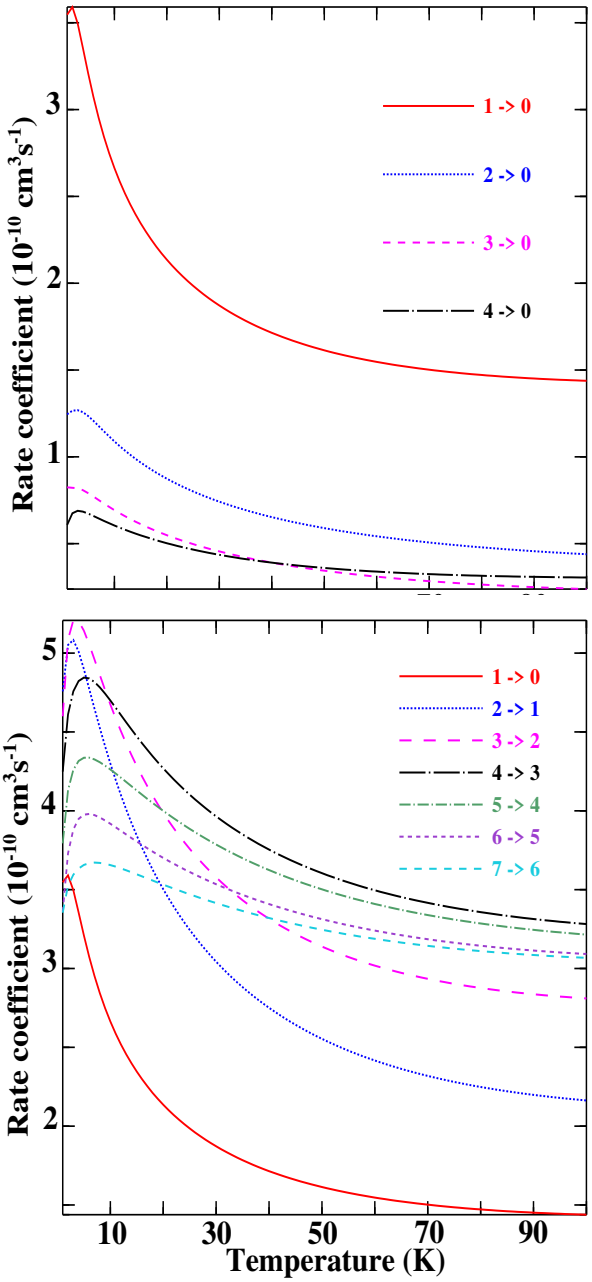

Figure 4. Downward rate coefficients of NS^+ induced by collision with para-$H_2(j = 0)$ as a function of the kinetic temperature. The upper (lower) panel displays the $j \longrightarrow 0$ ($\Delta j = 1$) transitions.

species. In this realm, it would be interesting to recompute the NS^+ abundance using the rates presented in this paper.

4 CONCLUSION

State-to-state inelastic cross sections of NS^+ induced by collision with para-H_2 have been computed by mean of the exact close coupling quantum mechanical approach in the total energy range [1.7-1,400 cm^{-1}]. These cross sections were thereafter thermally averaged using the velocity distribution of Maxwell-Boltzmann to obtain rate coefficients involving the 23 low-lying rotational levels for kinetic temperatures up to 100 K. The hyperfine rate coefficients were also calculated using the methodology established by Faure & Lique (2012). Indeed, these dynamic results were governed by the interaction potential of NS^+ and H_2 which was calculated with a high accurate ab initio level of theory, namely explicitly correlated coupled cluster with single, double and non-iterative triple excitation connected to the augmented–correlation consistent–polarized valence triple zeta Gaussian basis set.

The effect of the H_2 approach (this work) towards NS^+ was compared to that of He (Cabrera-González et al. 2018; Trabelsi et al. 2018). In terms of electron interactions, differences are observed mainly for the well depths. This has led to a wider range of resonances for the cross sections induced by para-$H_2(j = 0)$ collision than for those due to He impact. The influence on the rate coefficients concerns mainly the lower temperatures where different behaviors are noted. As overall, the rate coefficients, with and without hyperfine splitting, computed in this work are 1.5–4 times larger than those due to He impact. Nevertheless, reasonable agreements are observed in terms of shape, leading to the same propensity rules.

Through the discussion made along this paper, it is obvious that recomputing the abundance of NS^+ using the data presented here will significantly improve the value reported in the literature. Moreover, we expect that this paper will encourage similar investigations on the [N,S]-bearers. For example, considering the full 4D-PES of the H_2-NS^+ complex in order to explicitly treat the para-$H_2(j = 0)$-NS^+ and ortho-$H_2(j = 1)$-NS^+ rate coefficients.

Table 3. Close coupling rotational rate coefficients (in unit of $10^{-10} cm^3 s^{-1}$) of NS^+ due to both para-$H_2(j = 0)$ and He. The brackets stand for the ratios of the rate coefficients (NS^+–para-$H_2(j = 0)$/NS^+–He).

j → j'	T = 10 K		T = 20 K		T = 50 K		T = 100 K	
1 → 0	0.86[a]	2.66	0.76[a]	2.14	0.67[a]	1.61	0.68[a]	1.44
	(3.09)		(2.81)		(2.40)		(2.12)	
2 → 1	1.46[a]	4.30	1.29[a]	3.50	1.12[a]	2.55	1.12[a]	2.16
	(2.94)		(3.71)		(2.77)		(1.93)	
3 → 2	1.55[a]	4.67	1.41[a]	3.99	1.25[a]	3.14	1.23[a]	2.81
	(3.01)		(2.83)		(2.51)		(2.28)	
5 → 4	1.43[a]	4.26	1.34[a]	4.00	1.24[a]	3.50	1.25[a]	3.21
	(2.98)		(2.98)		(2.82)		(2.57)	
6 → 5	1.33[a]	3.92	1.27[a]	3.70	1.20[a]	3.31	1.23[a]	3.09
	(2.95)		(2.91)		(2.76)		(2.51)	

[a] stands for Trabelsi et al. (2018)

Table 4. Hyperfine rate coefficients (in unit of $10^{-11} cm^3 s^{-1}$) of NS^+ due to both para-$H_2(j = 0)$ and He. The brackets stand for the ratios of the hyperfine rate coefficients (NS^+–para-$H_2(j = 0)$/NS^+–He).

j, F → j', F'	T = 10 K		T = 50 K		T = 100 K	
1, 0 → 0, 1	9.01[a]	26.64	6.77[a]	16.14	6.80[a]	14.38
	(2.96)		(2.38)		(2.11)	
1, 0 → 1, 2	3.47[a]	10.66	4.33[a]	10.25	5.58[a]	8.18
	(3.07)		(2.36)		(1.47)	
1, 2 → 1, 1	1.56[a]	4.80	1.95[a]	4.60	2.51[a]	3.68
	(3.07)		(2.36)		(1.47)	
2, 1 → 0, 1	2.94[a]	10.89	1.87[a]	5.89	2.03[a]	4.39
	(3.70)		(3.15)		(2.16)	
2, 1 → 2, 3	0.59[a]	1.91	2.23[a]	6.21	2.45[a]	6.56
	(3.24)		(2.78)		(2.68)	
2, 3 → 2, 1	0.25[a]	0.82	0.95[a]	2.66	1.05[a]	2.81
	(3.28)		(2.80)		(2.68)	

[a] stands for Cabrera-González et al. (2018)

AKNOWLEDGEMENTS

The author warmly acknowledges many conversions with Pr. F. Lique (LOMC, France) and Pr. K. Hammami (LSAMA, Tunisia). This work has been supported by the Abdus Salam International Center for Theoretical Physics, Office of External Activities (ICTP-OEA) under the NET45 program.

REFERENCES

Ajili Y., Abdallah D. B., Al-Mogren M. M., Lique F., Francisco J., Hochlaf M., 2016a, Physical Review A, 94, 012512
Ajili Y., Abdallah D. B., Al-Mogren M. M., Francisco J., Hochlaf M., 2016b, Monthly Notices of the Royal Astronomical Society, 458, 1581
Arthurs A., Dalgarno A., 1960. pp 540–551
Bop C. T., Hammami K., Niane A., Faye N., Jaïdane N., 2016, Monthly Notices of the Royal Astronomical Society, p. stw2809
Bop C. T., Hammami K., Faye N., 2017, Monthly Notices of the Royal Astronomical Society, 470, 2911
Bop C. T., Faye N., Hammami K., 2018, Monthly Notices of the Royal Astronomical Society, 478, 4410
Boys S. F., Bernardi F. d., 1970, Molecular Physics, 19, 553
Brünken S., Yu Z., Gottlieb C., McCarthy M., Thaddeus P., 2009, The Astrophysical Journal, 706, 1588
Cabrera-González L., Mera-Adasme R., Páez-Hernández D., Denis-Alpizar O., 2018, Monthly Notices of the Royal Astronomical Society, 480, 4969
Cernicharo J., et al., 2018, The Astrophysical Journal Letters, 853, L22
Daniel F., et al., 2013, Astronomy & Astrophysics, 560, A3
Daranlot J., Hincelin U., Bergeat A., Costes M., Loison J.-C., Wakelam V., Hickson K. M., 2012, Proceedings of the National Academy of Sciences, 109, 10233
Denis-Alpizar O., Kalugina Y., Stoecklin T., Vera M. H., Lique F., 2013, The Journal of chemical physics, 139, 224301
Dubernet M.-L., Grosjean A., 2002, Astronomy & Astrophysics, 390, 793
Dumouchel F., Kłos J., Lique F., 2011, Physical Chemistry Chemical Physics, 13, 8204
Dunning Jr T. H., 1989, The Journal of chemical physics, 90, 1007
Durig J. R., Zheng C., Deeb H., 2006, Journal of molecular structure, 784, 78
Dyke J., 1977, J. Chem. Sot. Faraday Trans. II, 73, 147
Faure A., Lique F., 2012, Monthly Notices of the Royal Astronomical Society, 425, 740
Frerking M., Linke R., Thaddeus P., 1979, The Astrophysical Journal, 234, L143
Goldflam R., Kouri D., Green S., 1977, The Journal of Chemical Physics, 67, 5661
Gottlieb C., Ball J., Gottlieb E., Lada C., Penfield H., 1975, The Astrophysical Journal, 200, L147
Halfen D., Ziurys L. M., Brünken S., Gottlieb C., McCarthy M., Thaddeus P., 2009, The Astrophysical Journal Letters, 702, L124
Hernández Vera M., Lique F., Dumouchel F., Hily-Blant P., Faure A., 2017, Monthly Notices of the Royal Astronomical Society, 468, 1084
Huber K.-P., 2013, Molecular spectra and molecular structure: IV. Constants of diatomic molecules. Springer Science & Business Media
Hutson J., Green S., 1994, Collaborative computational project
Irvine W. M., Senay M., Lovell A. J., Matthews H. E., McGonagle D., Meier R., 2000, Icarus, 143, 412
Kłos J., Lique F., 2008, Monthly Notices of the Royal Astronomical Society, 390, 239
Knizia G., Adler T. B., Werner H.-J., 2009, The Journal of Chemical Physics, 130, 054104
Krupa J., Wierzejewska M., 2016, Chemical Physics Letters, 652, 46
Kuiper T., Zuckerman B., Kakar R., Rodriguez Kuiper E., 1975, The Astrophysical Journal, 200, L151
Laas J. C., Caselli P., 2019, arXiv preprint arXiv:1903.01232
Lanza M., Kalugina Y., Wiesenfeld L., Lique F., 2014a, The Journal of chemical physics, 140, 064316
Lanza M., Kalugina Y., Wiesenfeld L., Faure A., Lique F., 2014b, Monthly Notices of the Royal Astronomical Society, 443, 3351
Li H., Roy P.-N., Le Roy R. J., 2010, The Journal of chemical physics, 133, 104305
Lique F., Toboła R., Kłos J., Feautrier N., Spielfiedel A., Vincent L., Chałasiki G., MH A., 2008, Astronomy & Astrophysics, 478, 567
Manolopoulos D., 1986, The Journal of chemical physics, 85, 6425
McGonagle D., Irvine W. M., 1997, The Astrophysical Journal, 477, 711
Meyer D. M., Cardelli J. A., Sofia U. J., 1997, The Astrophysical Journal Letters, 490, L103
Monteiro T., 1985, Monthly Notices of the Royal Astronomical Society, 214, 419
Nguyen M. T., Vanquickenborne L. G., Flammang R., 1994, The Journal of chemical physics, 101, 4885
Pereira P. S., Macedo L. G., Pimentel A. S., 2009, The Journal of Physical Chemistry A, 114, 509
Prasad S. S., Huntress Jr W. T., 1982, The Astrophysical Journal, 260, 590
Sahnoun E., Nkem C., Nainbounda A., Hammami K., Jaïane N., Owono L. O., 2018, Astrophysics and Space Science, 363, 195
Tieftrunk A., Pineau des Forets G., Schilke P., Walmsley C., 1994, Astronomy and Astrophysics, 289, 579
Trabelsi T., Ajili Y., Hammami K., Mogren Al Mogren M., Francisco J., Hochlaf M., 2018, Monthly Notices of the Royal Astronomical Society, 480, 4259
Wakelam V., Caselli P., Ceccarelli C., Herbst E., Castets A., 2004, Astronomy & Astrophysics, 422, 159
Walker K. M., Lique F., Dumouchel F., Dawes R., 2016, Monthly Notices of the Royal Astronomical Society, 466, 831
Werner H.-J., et al., 2010, See http://www. molpro. net
Wierzejewska M., Moc J., 2003, The Journal of Physical Chemistry A, 107, 11209